Journal of Theoretical and Applied Physics (2018) 12:243–248
https://doi.org/10.1007/s40094-018-0310-3

RESEARCH

Magnetoresistance temperature dependence of LSMO and LBMO perovskite manganites

Z. Jafari Razi[1] · S. A. Sebt[1] · A. Khajehnezhad[1]

Received: 2 July 2018 / Accepted: 15 November 2018 / Published online: 4 December 2018

Abstract
$La_{0.7}Sr_{0.3}MnO_3$ (LSMO) and $La_{0\cdot7}Ba_{0.3}MnO_3$ (LBMO) Polycrystalline manganite nanoparticles were prepared by combustion method using glycine fuel. The ignition process was done at 360 °C and 330 °C for LSMO and LBMO, respectively. Both of the samples have rhombohedral structure using XRD analysis. The reduction is observed in electrical resistivity when external magnetic field is applied during the decrease in temperature from 300 to 89 °K, which is due to the tunneling between particles. The magnetoresistance (MR) of samples was measured in this range of temperature in both the presence and absence of a magnetic field of about 10 kG. The colossal role of a kind of extrinsic MR which is 19% and 22% for LSMO and LBMO, respectively, has been investigated in this research. The metal–insulator transition temperature of 200 °K is recorded for LBMO.

Keywords Manganites · Magnetoresistance · Low temperature · Combustion method

Introduction

In recent decades, a wide range of researches have been conducted on manganese oxide compounds with perovskite structure called manganite with chemical formula of $REMnO_3$ (RE: trivalent rare-earth ion like La, Pr, Sm & Nd). This structure is an antiferromagnetic insulator [1] and what makes it considerable is the mixed valence manganites with general structure of $RE_{1-x}AE_xMnO_3$ (AE: divalent alkaline-earth ion like Sr, Ca, Ba, etc.) which is practical in many different fields of industrial technology [2]. Actually, the $REMnO_3$ has an orthorhombic distortion and after substitution into specific ratio ($RE_{1-x}AE_xMnO_3$), the distortion transforms to the rhombohedral one which is better than the orthorhombic in structural, electrical and magnetic properties [2, 3]. These materials show many phenomenon, such as colossal magnetoresistance CMR [2] and magneto caloric effect MCE [4], which recently is massively attractive in technical field and have potential applications in solid oxide fuel cells [5], magnetic sensors [6], spintronic [6], biomedical field [3] and magnetic refrigeration technology [4]. The MR is defined as changing the resistance (resistivity) in the presence of applied magnetic field, and its percentage is obtained by equation [1] where R_H and R_0 are the resistance (resistivity) in the presence and absence of magnetic field, respectively.

$$\left[\frac{R_H - R_0}{R_0}\right] \times 100 \quad (1)$$

In manganites, there are two types of MRs. CMR occurs in high magnetic field (several Tesla) at room temperature due to intrinsic properties of single crystalline manganites. LFMR occurs in low magnetic field at a range of temperatures and depends on extrinsic properties of polycrystalline manganites like the method of preparation [7–10].

The intrinsic MR of manganites leads to decrease in resistance due to suppression of spin fluctuations in applied magnetic field. As this type of MR needs high magnetic fields, the practical applications of this effect are restricted. The extrinsic MR which is because of the existence of intergrain spin polarized tunneling (SPT) or spin-dependent scattering (SDS) between the grain boundaries in the presence of external magnetic field can be increased as the particles size decrease [8], or another elements are doped in manganites [11]. In fact, external factors such as preparation method, sintering temperature and particle morphology are of major

✉ S. A. Sebt
sa.sebt@srbiau.ac.ir

[1] Department of Physics, Science and Research Branch, Islamic Azad University, Tehran, Iran

impacts on grain boundaries which are the main reasons for extrinsic MR effect [10, 12–14].

Among $RE_{1-x}AExMnO3$ compounds, $La_{1-x}AExMnO3$ (AE = Sr, Ca, Ba) were analyzed both experimentally and theoretically in recent years [15]. According to these analyses around $x \sim 0.3$ these materials are in metal ferromagnetic phase, and at lower and higher than $x \sim 0.3$ they are antiferromagnetic insulators [15].

There are several methods, such as milling [16], sol–gel [4], solid state reaction [8] and combustion [3], through which manganites are prepared. These routes have some drawbacks such as complex procedures, long reaction time and very high temperatures requirement. The combustion rout which we applied in this work is economic and time-saving. During this process, there is no gases generation and particle size growth. In fact, it is a popular method for nanomaterials [3, 17, 18]. The main purpose of this research is the substitution of divalent atoms with different atomic radius for La in $La_{1-x}AExMnO3$, which affects the magnetic and electrical properties of it [19–21]. As a result, La0.7Sr0.3MnO3 (LSMO) and La0.7Ba0.3MnO3 (LBMO) were prepared, and their structural and magnetoresistance properties were analyzed. As well as this, applying combustion method for LBMO synthesis is the outstanding aspect of this research.

Experimental details

LSMO and LBMO were synthesized by the combustion method using nitrates such as La(NO3)3·6H2O, Mn(NO3)2·4H2O, Sr(NO3)2 and Ba(NO3)2 as the initial ingredients and glycine as a fuel [3, 18]. The process consists of two steps. Firstly, the stoichiometric amounts of the nitrates, including La(NO3)3·6H2O,Mn(NO3)2·4H2O and Sr(NO3)2 for LSMO, La(NO3)3.6H2O, Mn(NO3)2.4H2O and Ba(NO3)2 for LBMO and glycine, were dissolved separately in distilled water and formed the uniform solution using magnetic stirrer. Then, the uniform evaporated gel of primary materials was formed keeping the product on magnetic stirrer for 30 min at 100 °C. Following which, the temperature was enhanced gently so as to ignition takes place. The ignition occurred during the sintering process with a voluminous and high speed flame at 360 °C for LSMO and 330 °C for LBMO. Finally, the fluffy blackish or dark brown powder of LSMO and LBMO obtained as final product along with brown vapor of nitrogen dioxide which is due to the decomposition of nitrates releasing CO2 and O2 gases. The prepared LSMO and LBMO powder were sintered at 900 °C for 5 h, while the powder was pelletized by pressing at 10 ton pressure.

The combustion reaction for LSMO is given below [3]:

$$0.7La^{3+}\left(NO_3\right)_3^{3-} + 0.3Sr^{2+}\left(NO_3\right)_2^{2-} + Mn^{2+}\left(NO_3\right)_2^{2-} + 2.54\left(NH_2 - CH_2 - COOH\right) + 1.33O_2 \rightarrow La_{0.7}Sr_{0.3}MnO_3 + 6.35H_2O + 3.62N_2 + 5.08CO_2$$

In the present work, the LBMO combustion reaction was also carried out like the above reaction adding barium nitrate instead of strontium nitrate with the same amount of glycine fuel. The stoichiometric amounts of nitrates and glycine, respectively, as an oxidizing (O) and a reducing agent (F), were used. These amounts are calculated based on total oxidizing and reducing valences of O and F. The equivalence ratio of O/F acts as an essential numerical coefficient in combustion process. When it becomes unity, heat is released at its maximum level [18, 22]. This kind of combustion is called stoichiometric one [3, 18, 23]. Using appropriate fuel as an agent has very important role in both the temperature of decomposition and extension of CO_2 and H_2O gases. Glycine fuel as a soluble amino acid in water makes it possible for metal ions to compound in the solution. It is an affordable and available material. It causes gradients to precipitate simultaneously during the combustion [3, 18].

X-ray diffraction (XRD) patterns were recorded for structural analyzing by X'Pert PRO MPD model using Cu-Kα radiation in the 2θ range of 20° to 80° with the wave length of 1.5406Å, voltage of 40 kV, current of 40 mA. The results were analyzed with Rietveld refinement by Maud software. Fourier transform-Infrared (FT-IR) analyses were carried out by a thermo Nicolet, (Model Nexus No. 870, USA) in the range of 400–4000 cm^{-1} in order to checking chemical bonding of the material. The compositional analyses were done by Energy-dispersive analysis of X-ray spectroscopy (EDAX) using Philips XL30. The surface morphology and elemental detection were recorded with a KYKY-EM3200 model of scanning electron microscope (SEM). The resistivity measurements were done by four-point probe method in a magnetic field of 10 kG at low temperatures to 89 °K.

Results and discussion

Figure 1 shows the X-ray diffraction of LSMO and LBMO samples after sintering at 900 °C. Both of polycrystalline samples have phase purity. It indicates that samples have the rhombohedral structure with $R\bar{3}c$ space group. It is confirmed by Rietveld refinement in Fig. 2.

Figure 3 indicates the SEM images of samples after sintering at 900 °C. As the images show, most of LSMO particles have coalesced. Grain boundaries of LSMO are narrower than that of LBMO.

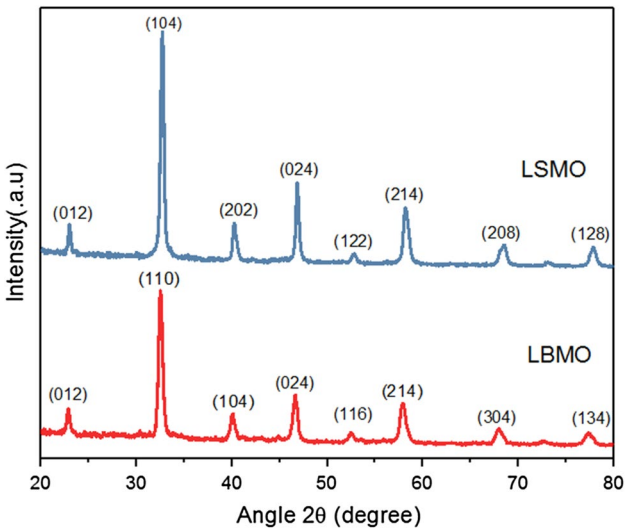

Fig. 1 XRD patterns of the LSMO and LBMO sintered at 900 °C

The results of XRD and Rietveld refinement are summarized in Table 1. The lattice parameters of LBMO specially the *c* is larger than that of LSMO. One reason would be the substitution of Ba as a divalent atom with different atomic radius with respect to Sr, which increases the lattice parameter of the structure.

EDAX was carried out for quantitative elemental analysis of the compounds. The spectra are shown in Fig. 4. It shows that both samples have elemental signals which are close to their stoichiometric values. Figure 3 indicates the SEM images of LBMO and LSMO samples respectively after sintering at 900 °C. Also there is no type of impurity.

The FT-IR spectra of samples sintered at 900 °C are shown in Fig. 5. The characteristic band of both samples is observed around 600 cm^{-1} which corresponds to Mn–O. This indicates that both samples strongly contain the metal–oxygen bonds which are due to the change in Mn–O–Mn bond length because of internal motion that causes stretching mode [3, 18, 24]. Peaks of 1074 and 1426 cm^{-1} correspond to $Sr(NO_3)_2$ in LSMO and $Ba(NO_3)_2$ in LBMO samples, respectively. O–H stretching vibrations and surface-adsorbed water on the nanoparticles of LSMO and LBMO bring about peaks around 2917 and 3854 cm^{-1} for both samples [3, 18].

The temperature dependence of the resistivity of LSMO and LBMO polycrystalline samples both in the absence and the presence of 10 kG applied magnetic field in the temperature range from 89 to 300 °K is shown in Fig. 6. The results

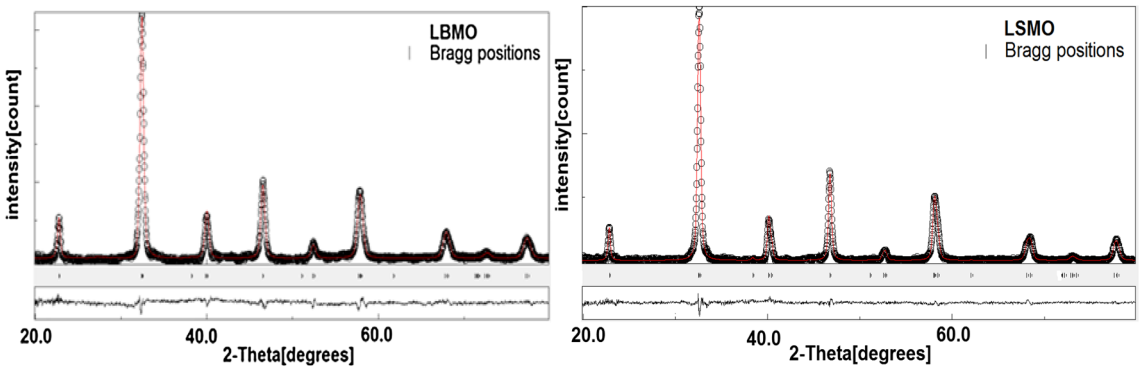

Fig. 2 The Rietveld refinement analysis of the XRD pattern for LSMO and LBMO samples

Fig. 3 SEM images of nanoparticles

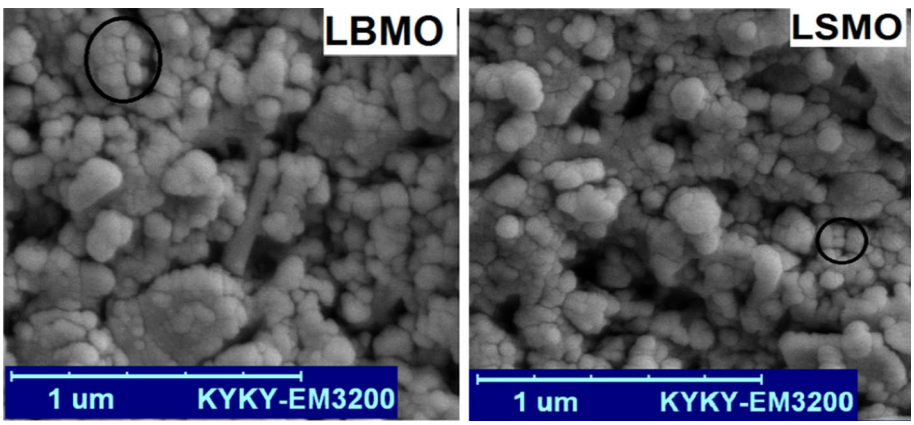

Table 1 Structural details

Sample	FWHM	*a* (Å)	*c* (Å)
LSMO	0.48996	5.502905	13.377431
LBMO	0.44326	5.509113	13.553258

have been shown that the metal–insulator transition (T_{MI}) for LBMO occurs around 200 °K, where its metallic and insulating behavior is separated [12, 25]. It has been shown that by decreasing the temperature from 300 to 200 °K the resistivity of LBMO sample increases and as it drops further to 89 °K the resistivity decreases. Wider grain boundaries in LBMO above 200 °K might be the reason why it is insulated at these temperatures.

However, for LSMO sample, its resistivity decreases with the drop of temperature and in the range of 89–300 °K there is no transition up to temperatures higher than the room temperature [26]. As at temperatures below 300 K, the particles are closer and grain boundaries are narrower, which is observed in SEM analyses, it is highly likely to more electrons tunneling occurs, through which the resistivity decreases and metal behaviors appear. Also applying magnetic field of 10 kG leads to decrease in the resistivity of both samples. Furthermore, Ba doping in LMO increases the resistivity comparing with Sr doping [10, 25]. At low temperatures together with the presence of the magnetic field, the decrease in resistivity is more in comparison with the absence of it. T_{MI} in mixed valence manganites is explained by double exchange (DE) interaction which is a type of magnetic exchange interaction between ions in different oxidation state [12]. In DE interaction, first an electron, among those which are all parallel spin-up, transfers from Mn^{3+} to oxygen ion and from it to Mn^{4+} ion simultaneously which is

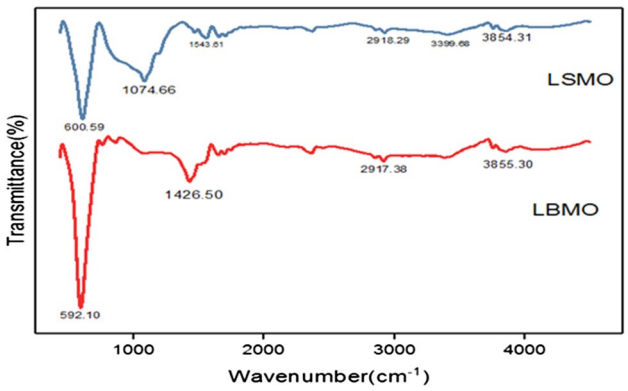

Fig. 5 FTIR spectra of LSMO and LBMO

based on bond length of Mn–O–Mn. This interaction is the reason for metallic ferromagnetic behavior [12].

In Fig. 7, MR as a function of temperature is illustrated at the range of temperature from 89 to 300 °K under external magnetic field of 10 kG. MR value of polycrystalline samples, in the presence of external magnetic field, increases with temperature reduction which is due to SPT or SDS across the grain boundaries as the electron flows across grain boundaries, which in fact is similar to the sandwiching of a very thin layer of insulating between the two ferromagnetic layers as ferromagnetic tunnel junction. In this case, the grain boundaries play the role of insulating layer through which the electron hopping. This electron is in correlation with such sandwiching layer and also the spin states of the neighbor magnetic layers [27, 28]. MR value is 3% at 300 °K and 22% at 89 °K for LSMO and 4% at 300 °K and 19% at 89 °K for LBMO samples. The percentage of magnetoresistance in LBMO prepared by the combustion method is 10%

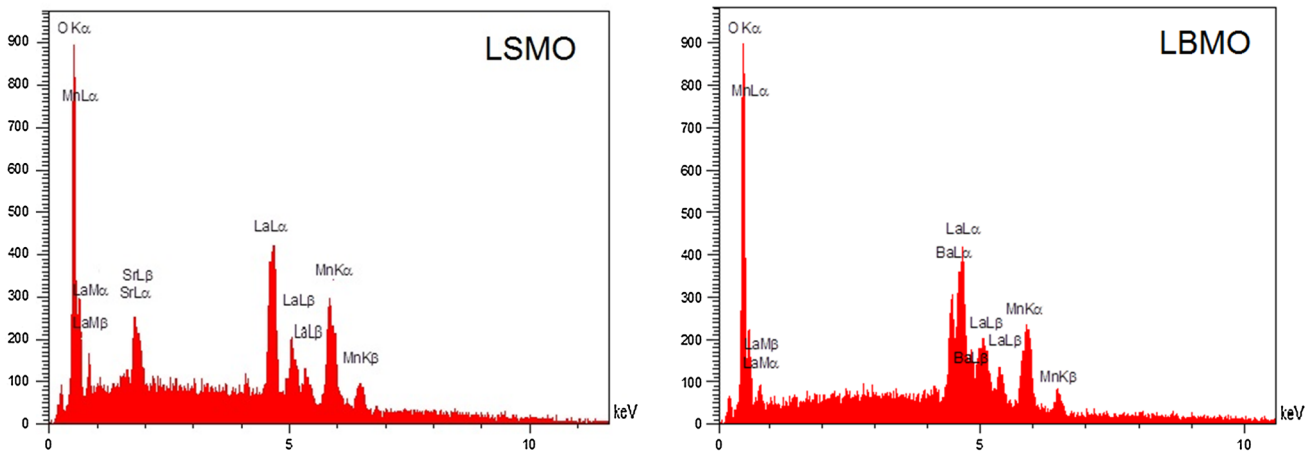

Fig. 4 EDAX spectra of LSMO and LBMO nanoparticles

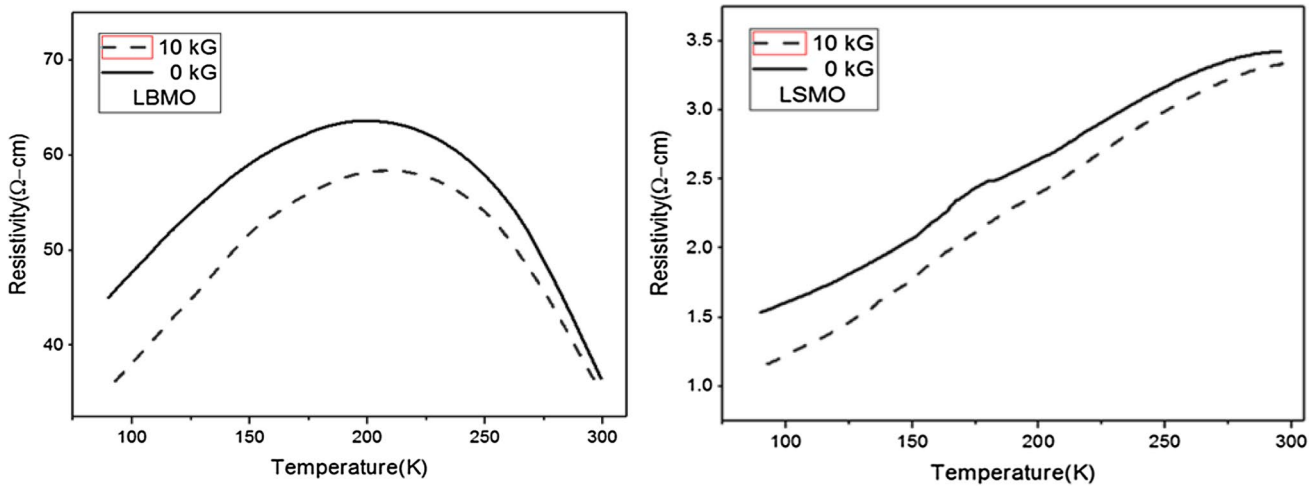

Fig. 6 Variation of resistivity of LSMO and LBMO with temperature in the absence and presence of the magnetic field

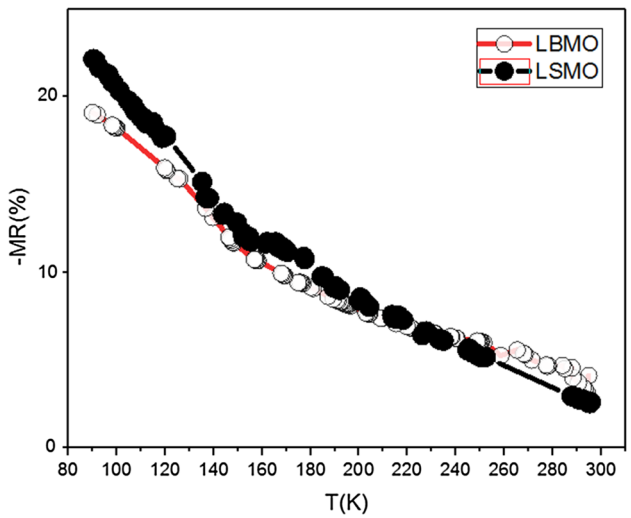

Fig. 7 MR curve of LSMO and LBMO

in 100 °K, which is higher than that of the sample prepared by the sol–gel method [29].

Conclusions

In conclusion, LBMO, for the first time, and LSMO polycrystalline nanoparticles were prepared by combustion method using glycine as a fuel. The TMI of LBMO is 200 °K, and there is no transition temperature for LSMO in this temperature range. MR of LSMO and LBMO, at 89 °K, is 22% and 19%, respectively. As the temperature declines in the presence of the external magnetic field, so does the resistivity. With decrease in electrons scattering, in the presence of magnetic field, electrical resistivity decreases (MR is negative) and this effect is due to the ordered alignment of spins in grain boundaries in the presence of the magnetic field. Therefore, as the intensity of magnetic field increases, so does the amount of MR.

References

1. Supelano, G., et al.: Effect of Mg addition on $LaMnO_3$ ceramic system. J. Mater. Res. Technol. **7**, 77–81 (2017)
2. Huang, Y.-H., et al.: Structural dependence of magnetic and transport properties in doped manganite perovskites. Chin. J. Struct. Chem. **21**, 233–240 (2002)
3. Thorat, N.D., et al.: Polyvinyl alcohol: an efficient fuel for synthesis of superparamagnetic LSMO nanoparticles for biomedical application. Dalton Trans. **41**, 3060–3071 (2012)
4. Winarsih, S., et al. Electrical properties of $La_{0.7}Ba_{0.297}Ca_{0.003}MnO_3$ obtained by low temperature sol-gel synthesis. ISCPMS, 2016. In: AIP Conference, vol. 1862, pp. 030044-1–030044-5 (2016)
5. Miyamaru Seo, E.S., et al.: Properties of sr-doped lanthanum manganites for SOFC. Mater. Sci. Forum. **416–418**(1), 354–358 (2003). https://doi.org/10.4028/msf.416-418.354
6. Yunhui, X., et al.: Magnetic field sensors from polycrystalline manganites. Sens. Actuators A **91**(1–2), 26–29 (2001). https://doi.org/10.1016/S0924-4247(01)00493-9
7. Ravi, V., et al.: Synthesis of $La_{0.7}Sr_{0.3}MnO_3$ at 800 C using citrate gel method. Ceram. Int. **33**, 1129–1132 (2007)
8. Kameli, P., et al.: Influence of grain size on magnetic and transport properties of polycrystalline $La_{0.8}Sr_{0.2}MnO_3$ manganites. J. Alloys Comp. **450**, 7–11 (2008)
9. Zhao, L.F., et al.: Low field magnetoresistance observed in polycrystalline $La_{0.67}Ca_{0.33}Mn_{1-x}O_3$ sintered at low temperature. Mater. Sci. Eng. B **127**, 193–197 (2006)

10. Lim, K.P., et al.: Effect of divalent Ions (A = Ca, Ba and Sr) substitution in La-A-Mn-O manganite on structural, magnetic and electrical transport properties. Am. J. Appl. Sci. **6**(6), 1153–1157 (2009)
11. Lopez, M.A., et al.: Intergranular magnetoresistance in nanomanganites. Nanotechnology **14**, 212–219 (2003)
12. Winarsih, S., et al.: The effect of Ca-doping on structure and microstructure of $La_{0.7}(Ba_{1-x}Ca_x)_{0.3}MnO_3$. AIP Conf. Proc. **2017**, 030044-1–030022-5 (1862)
13. Gaur, A., et al.: Study of structural, magnetic and magneto-transport properties of nanocrystalline $La_{2/3}Ca_{1/3}MnO_3$ manganite. J. Optoelectron. Adv. Mater. **4**(7), 989–994 (2010)
14. Hwang, H.Y., et al.: Spin-polarized intergrain tunneling in $La_{2/3}Sr_{1/3}MnO_3$. Phys. Rev. Lett. **77**, 2041–2044 (1995)
15. Haghiri-Gosnet, A.-M., Renard, J.-P., et al.: TOPICAL REVIEW CMR manganites: physics, thin films and devices. J. Phys. D: Appl. Phys **36**, R127–R150 (2003)
16. Xiong, C.S., et al.: A modified synthesis method of manganese perovskite $La_{0.7}Ca_{0.3}MnO_3$ by high energy ball milling and post heat treatment. Mater. Res. Bull. **42**, 904–911 (2007)
17. Solanki, P.S., et al.: Structural, microstructural, transport, and magnetotransport properties of nanostructured LSMO manganites. J. Mater. Res. **25**, 1799–1802 (2010)
18. Shinde, K.P., et al.: Combustion synthesis and characterization of perovskite $La_{0.9}Sr_{0.1}MnO_3$. Mater. Chem. Phys. **134**, 881–885 (2012)
19. Wang, T., et al.: Mechanochemical effects on microstructure and transport properties of nanocrystalline $La_{0.8}Na_{0.2}MnO_3$ ceramics. J. Alloys Comp. **458**, 248–252 (2008)
20. Kalyana Lakshmi, Y.K., Venkataiah, G., Vithaland, M., Venugopal Reddy, P.: Magnetic and electrical behavior of La1−xAxMnO3 (A=Li, Na, K and Rb) manganites. Phys. B. **403**, 3059–3066 (2008)
21. Im, H.S., Chon, G.B., Lee, S.M., Koo, B.H., Leeand, C.G., Jung, M.H.: Preparation and characterization of $La_{0.7}AE_{0.3}MnO_3$ (AE= Ca, Sr, Ba): perovskite structured manganites. J. Magnet. Magnet. Mater. **310**, 2668–2670 (2007)
22. Jain, S.R., et al.: A new approach to thermochemical calculations of condensed fuel-oxidizer mixtures. Combust. Flame **40**, 71–79 (1981)
23. Shinde, K.P., et al.: Solution-combustion synthesis of $La_{0.65}Sr_{0.35}MnO_3$ and the magnetocaloric properties. Mater. Sci. Eng. B **167**, 202–205 (2010)
24. Gao, F., et al.: Far-infrared reflection and transmission of $La_{1-x}Ca_xMnO_3$. J. Alloys Compd. **347**, 314–318 (2002)
25. Kumar, R., et al.: Current-induced effect on resistivity and magnetoresistance of $La_{0.67}Ba_{0.33}MnO_3$ manganite. J. Magn. Magn. Mater. **320**, 2741–2745 (2008)
26. Singh, S. et al. Current-induced effect on resistivity and magnetoresistance of $La_{0.67}Ba_{0.33}MnO_3$ manganite (2017)
27. Sun, J.Z., Krusin-Elbaum, L., Duncombe, P.R., Gupta, A., Laibowitz, R.B.: Temperature dependent, non-ohmic magnetoresistance in doped perovskite manganate trilayer junctions. Appl. Phys. Lett. **70**, 1769 (1997)
28. Viret, M., Drouet, M., Nassar, J., Contour, J.P., Fermon, C., Fert, A.: Low-field colossal magnetoresistance in manganite tunnel spin valves. Europhys. Lett. **39**, 545–550 (1997)
29. Mohamed, A.E.M.A.: Magnetoresistive and magnetocaloric response of manganite/insulator system. J. Alloy. Compd. **657**, 495–505 (2016)